ACS Photonics

Letter

pubs.acs.org/journal/apchd5

Detecting Single Gold Nanoparticles (1.8 nm) with Ultrahigh-*Q* Air-Mode Photonic Crystal Nanobeam Cavities

Feng Liang and Qimin Quan*

Rowland Institute at Harvard University, 100 Edwin H. Land Boulevard, Cambridge, Massachusetts 02142, United States

Supporting Information

ABSTRACT: The growing applications of nanoparticles in energy and healthcare demand new metrology techniques with improved sensitivity, lower sample concentration, and affordable instrument cost. Here we demonstrate the first air-mode photonic crystal nanobeam cavity with ultrahigh *Q*-factor ($Q = 2.5 \times 10^5$) and ultrasmall mode volume ($V = 0.01\lambda^3$) at telecom wavelength. The air-mode cavity has strong field localization outside of its high-index material, thus significantly improving the sensitivity to detect nanoparticles. The strong field gradient attracts the nanoparticles to its field maximum, improving the detection efficiency. Combining these advantages, we report detecting and sizing single gold nanoparticles down to 1.8 nm in diameter (equivalently single polystyrene nanoparticle of 3 nm in diameter) with significantly reduced sample concentration (~fM) than traditional optical techniques. In addition, the air-mode ultrahigh *Q*, ultrasmall *V* photonic crystal nanobeam cavity will be a useful platform to study strong light−matter interactions, nonlinear processes, and cavity quantum electrodynamics.

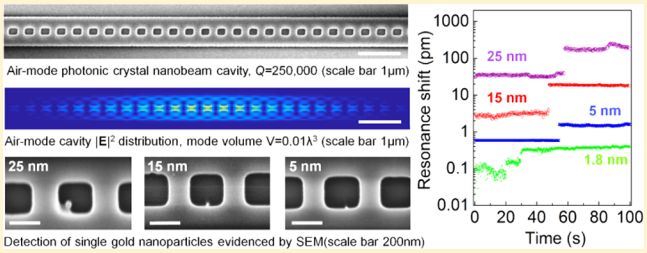

KEYWORDS: *photonic crystal nanobeam cavity, nanoparticle, optical force*

Nanotechnology has gained explosive growth in medical diagnostics and therapy,[1−3] energy,[4,5] and sensing[6] applications. For example, gold nanoparticles, widely used in cancer therapeutics, show critical efficacy dependence on their sizes: diameters of 2−6 nm have shown efficient penetration into the cell nucleus,[7] those of 6−10 nm were found to prefer peri-nuclear localization,[8] those of 50 nm showed optimal cellular uptake,[9,10] and those of 100−200 nm showed the highest possibility for long circulation in the body.[2] Existing optical techniques, such as dynamic light scattering (DLS) or UV−vis spectrometry require high concentrations (DLS, μM; UV−vis, nM) and large sample volumes (mL) and suffer from reliability issues when the sizes go below 10 nm.[11−13] Transmission or scanning electron microscopy, on the other hand, requires a strict laboratory environment and critical sample preparation and thus is not suitable when fast and frequent size analysis is required.

Optical nanocavities have shown great promise as an alternative metrology method to spectroscopy and imaging. Since the first demonstration of detecting a single virus (diameter about 100 nm)[14] with the whispering gallery mode (WGM) microcavities, follow-up progress has achieved detection of nanoparticles down to 20 nm.[15−22] Recently, the hybrid plasmonic WGM cavities further achieved detection of single proteins[23] and DNAs[24] (size ~5 nm). These cavities detect nanoparticles by measuring the resonance shift of the cavity mode induced by the nanoparticles.[25] This is now known as the reactive sensing mechanism, first demonstrated in detecting protein adsorptions on WGM surfaces.[26,27] When this mechanism is used to detect single nanoparticles, the resonance shift scales to the third order of the particle size and second order of the local field strength and inversely to the cavity mode volume ($V = \int \varepsilon|E|^2 \, dV/[\varepsilon|E|^2]_{max}$), in the regime where the nanoparticle has much smaller dimensions than the resonance wavelength. Other methods such as mode splitting[15] and mode broadening[19] have also been used to detect nanoparticles. In all cases, the detection limit is improved by large *Q*/*V* and large local field strength.[28] Photonic crystal cavities have potentially higher sensitivities than WGM cavities due to their small cavity *V* (typically 2 to 3 orders of magnitude smaller than WGM cavities). In addition, these cavities are fabricated using CMOS (complementary metal-oxide semiconductor)-compatible processes, thus opening up the possibility to integrate nanocavity arrays and on-chip photodetector arrays at high density for multiplexed sensing. However, detecting nanoparticles smaller than 25 nm has not been demonstrated in photonic crystals.[18,20,29] The challenge is to simultaneously achieve high *Q*, small *V*, and strong local optical field in one cavity. For example, a dielectric-mode photonic crystal cavity has an ultrahigh *Q* (~10^6); however, its optical field is localized inside the high-index material.[18,30] Air-slot photonic crystals have small mode volumes ($0.06\ \lambda^3/n_{water}^3$)[29] and strong field localization in the air region; however, the *Q*'s demonstrated were at most 12 000.[20,29,31] The air-mode photonic crystal nanobeam cavity has been demonstrated only at microwave

Received: October 20, 2015
Published: November 25, 2015

DOI: 10.1021/acsphotonics.5b00602
ACS Photonics 2015, 2, 1692−1697

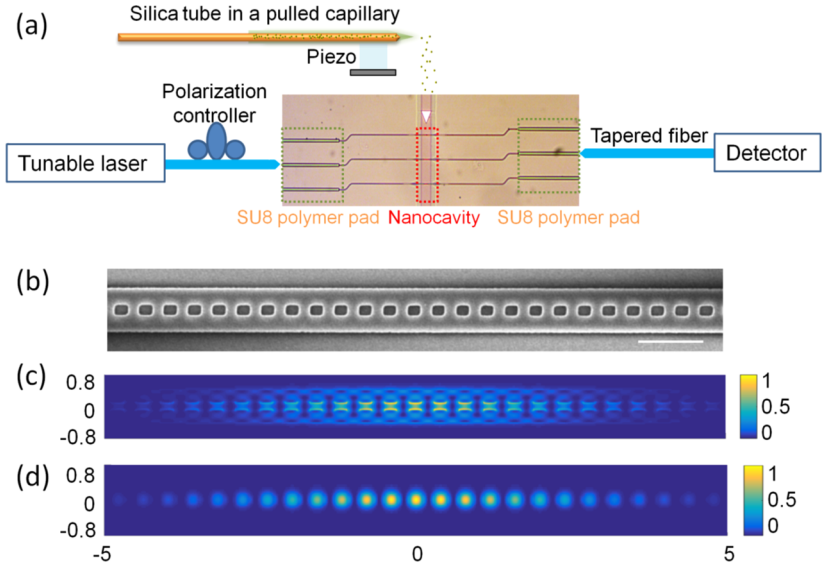

Figure 1. Photonic crystal nanobeam device and piezospray setup. (a) A tunable telecom laser was used to probe the cavity resonance from 1420 to 1520 nm. A tapered fiber coupled the signal from the laser to the SU8 polymer pad waveguide. The SU8 polymer pad converted its mode to the silicon waveguide mode and thus excited the cavity resonance mode. In the output, similarly, light transmitted through the nanobeam cavity was coupled to the silicon waveguide and the SU8 polymer pad, and finally collected by a tapered fiber to the photodetector. A polarization control unit was implemented to select the transverse electric polarization. A micropipet (end diameter of 100 μm) was actuated by a piezoelectric stack. The nanoparticles were delivered to the tip of the micropipet in methanol solution. (b) Scanning electron micrograph (SEM) image of the nanobeam cavity (top view, *xy* plane). (c and d) Electric field intensity ($|E|^2$) in the middle cut of the *xy* plane (c) and the *xz* plane (d). Scale bar: 1 μm.

frequencies (17.4 GHz) with a Q of 2.6×10^4.[32] Here we demonstrate the first air-mode photonic crystal nanobeam cavity at telecom wavelength (200 THz) with an ultrahigh Q (2.5×10^5) and small mode V ($0.01\ \lambda^3/n_{air}^3$). We used piezospray or electrospray to deliver individual nanoparticle aerosols to the cavity and improved the detection limit by an order of magnitude (down to 1.8 nm). Our method requires significantly reduced sample amounts (~500 nanoparticles per μL) and thus is uniquely suitable to detect trace amounts of nanoparticles.

RESULTS AND DISCUSSION

Air-Mode Photonic Crystal Nanobeam Cavity. The photonic crystal nanobeam cavities were fabricated in a silicon-on-insulator (SOI) platform. The device layer is 220 nm, and the oxide substrate is 2 μm. The nanobeam cavity consists of an array of rectangular gratings along a 800 nm wide silicon waveguide. The distance between two neighboring gratings is fixed at 400 nm; the width of each rectangular is fixed at 200 nm. The lengths of the rectangles are linearly increased from 220 to 240 nm from the middle of the nanobeam cavity to both its ends. This tapering geometry is optimized to create a hyperbolic potential for telecom photons, thus confining the optical energy to the middle of the structure with a Gaussian energy distribution.[33] The nanocavities were fabricated using a series of CMOS-compatible processes (see Supporting Information), including electron beam (ebeam) lithography and reactive ion etching. The SU8 pads were fabricated in a second ebeam lithography, aligned to the markers fabricated during the first ebeam process. The cavities were released from the substrate by etching off the silicon dioxide layer. The suspended geometry leads to increased Q-factors. We calculated the Q-factor of the current design to be 5×10^6 using the finite-difference time-domain (FDTD) simulation.

To characterize the photonic crystal nanobeam cavity, we used a tunable laser scanning from 1420 to 1520 nm (Santec S-band). As shown schematically in Figure 1a, a tapered optical fiber coupled the light from the laser to the SU8 pad. The polarization controller was used to launch the transverse electric polarization mode (matching the cavity mode polarization). A second tapered fiber was used to couple the light from the SU8 pad to the photodetector. The scanning electron micrograph (SEM) image of the nanobeam cavity is shown in Figure 1b (top image, *xy* plane), along with the $|E|^2$ distribution cut in the middle of the *xy* plane (Figure 1c) and *xz* plane (Figure 1d) obtained numerically by FDTD simulation. The fundamental mode exhibits an ultrahigh Q of 2.5×10^5, obtained by fitting to a Lorentzian profile. All the other modes in the band gap were measured to be in the range 10^3–10^5. The distinct feature of the air-mode cavity from the dielectric-mode cavity was manifested in Figure 2: the lower order cavity modes are observed at longer wavelengths and have higher Q's. This is because these cavity modes are originated from the Bloch mode at the air band edge.[34] The fundamental mode is pulled deeper into the band gap and thus has the lowest frequency, highest Q, and smallest V.

Single-Nanoparticle Detection. Here we set out to use the air-mode nanobeam cavity to detect single gold nanoparticles. As shown in Figure 1a, we used a piezoelectric actuator to drive a micropipet, one end of which was pulled to a diameter of ~100 μm. A silica tube (100 μm inside diameter, 190 μm outside diameter) was inserted into the micropipet from the nontapered end. The outlet of the tapered end was placed ~100 μm over the photonic crystal nanobeam cavity. The nanoparticles were diluted in methanol to ~1 fM, and a syringe pump was used to generate a constant flow of droplets. The piezoelectric stage was actuated at its resonance frequency (~20 kHz), generating an ultrasonic wave that vibrated individual nanoparticles into aerosols, subsequently evaporating and depositing them in the photonic crystal nanobeam cavity.

DOI: 10.1021/acsphotonics.5b00602
ACS Photonics 2015, 2, 1692–1697

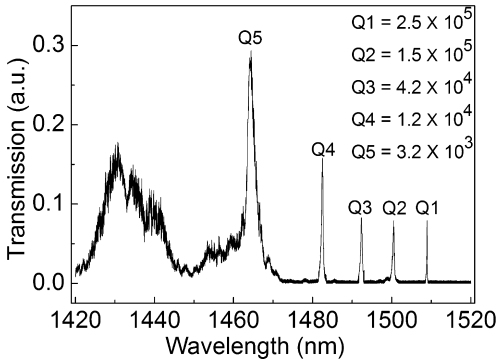

Figure 2. Resonance spectrum of an air-mode photonic crystal nanobeam cavity. Transmitted signal from the photonic crystal nanobeam cavity. The distinct feature of the air-mode cavity from the dielectric-mode cavity is shown: the lower order cavity modes were observed in the longer wavelength range and had higher Q's. The fundamental mode had a Q of 2.5×10^5, obtained from a numerical fit to a Lorentzian profile.

Supporting Information Figure S1a verifies that piezospray-deposited individual nanoparticles onto the silicon chip. Figure 3 exhibits the resonance jumps and Q drops when single gold nanoparticles of different sizes (1.8, 5, 15, and 25 nm) were deposited into the cavity. The devices were taken for SEM immediately after the discrete resonance jumps were observed. Figure 3a is plotted in log scale, since resonance shift scales with the diameter cubed. The baseline resonance is offset for easier visualization. Figure 3b plots the Q decrease, analyzed from the same measurements in Figure 3a. We found that Q drops were less sensitive than resonance jumps for small nanoparticles (e.g., 1.8 nm). Figure 4 shows the histograms of the resonances measured in Figure 3, for different nanoparticle sizes. Solid lines are normal distribution fitting curves. Defining the signal-to-noise ratio (SNR) as the shift of the normal distribution center divided by the average of the half-width-half-maxima of the two normal distributions, we obtained SNRs of 15, 19, and 10 for the cases of 5, 15, and 25 nm, respectively. We observed two resonance jumps for the 1.8 nm case, with SNRs of 1.4 and 4.

A common feature observed for all cases was that the nanoparticle was deposited in the center of the nanobeam cavity. To investigate this, we first carried out a finite element simulation (FEM) of the cavity-mode profile and the gradient force originated from the highly confined electromagnetic field. In all cases, the laser was continuously scanned at the proximity of the cavity resonance; therefore, the cavity was loaded during the experiment. Figure 5a visualizes the gradient force vectors derived from the fundamental cavity mode, which suggests that the gradient force would pull the nanoparticle into the center of the cuboid and push the nanoparticle to the side wall. As a control experiment, we piezosprayed the gold nanoparticles with the laser off. The nanoparticles were observed in the center cuboid of the cavity when the cavity resonance was excited (Figure 5b) and random places along the waveguide when the laser was off (Figure 5c). Given the electromagnetic field distribution, we can also calculate the strength of the gradient force trapping energy and compare it with the Brownian energy and potential energy (see Supporting Information). We note that trapping nanoparticles down to 18[35] and 80 nm[36] has been demonstrated in solution and in air, respectively, with a focused laser beam. The trapping energy in the current system is $U_{trap} \approx (2\pi R^3/\omega)P(Q/V)$, greatly enhanced by the ultrahigh Q/V. Here P is the output power, ω is the resonance frequency, and R is the radius of the nanoparticle. We estimated that for the case of a 5 nm nanoparticle and 1 mW input power, the trapping energy is $\sim 30 k_B T$, which overcomes the potential energy ($\sim 0.01 k_B T$) and the Brownian energy ($\sim k_B T$) at room temperature.

Second, we chose electrospray to deposit nanoparticles in the nanobeam cavity (see Supporting Information). As schematically shown in Figure 6a, 3 kV high voltage was applied between the 100 μm inner diameter electrospray probe and the silicon chip. The nanoparticles were carried in methanol (easy to evaporate) and were injected at 1 μL/min using a syringe pump. A 3 kV voltage was tested to be effective in generating a stable Taylor cone. The coulomb repulsive force turned big droplets into small aerosols, which was further nebulized by a

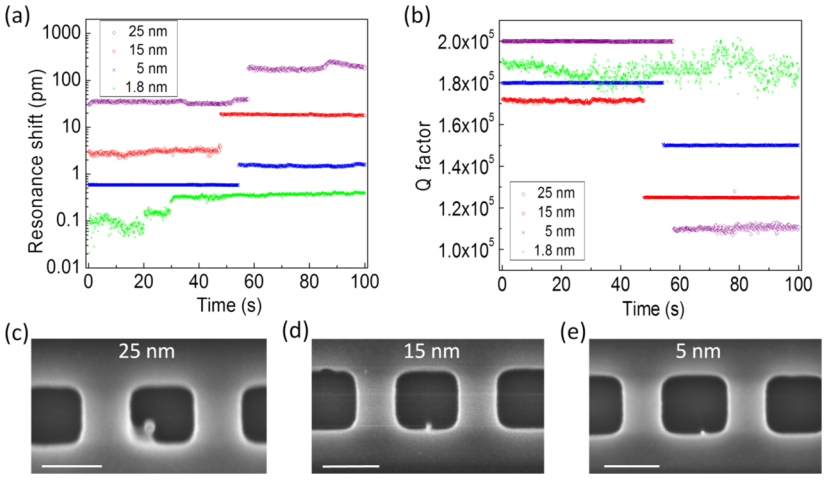

Figure 3. Observing single nanoparticles by monitoring the cavity resonance jumps and Q-factor drops. (a) Resonance shifts and (b) Q-factors measured in real time for different nanoparticle sizes (diameter 25, 15, 5, and 1.8 nm). Immediately after the resonance jumps were observed, the devices were taken for SEM (c–e). SEM images show single gold nanoparticle deposited inside the air-square region in the middle of the nanobeam cavity. The nanoparticles have diameters of 25 nm (c), 15 nm (d), and 5 nm (e), respectively. The 1.8 nm nanoparticle was not visible in SEM. Scale bar: 200 nm.

DOI: 10.1021/acsphotonics.5b00602
ACS Photonics 2015, 2, 1692–1697

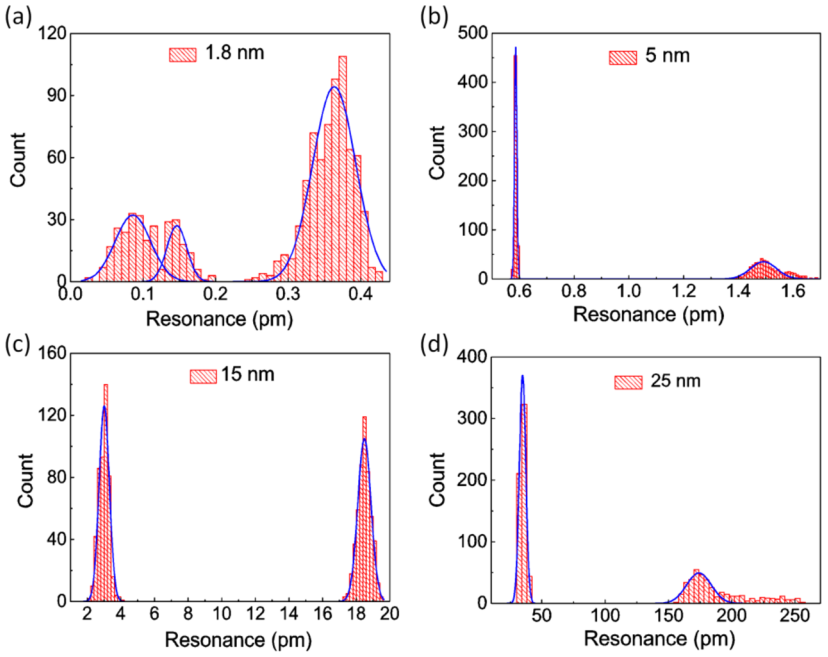

Figure 4. Histogram of the nanobeam cavity resonances. (a) Three normal distributions were identified, representing consecutive deposition of two nanoparticles (1.8 nm) into the cavity. The signal-to-noise ratios (SNR) of the two events are 1.4 and 4. SNR is defined as the resonance jump divided by the average of the two half-width-half-maxima of two normal distributions. (b) Single-nanoparticle (5 nm) deposition event with SNR = 15. (c) Single-nanoparticle deposition (15 nm) event with SNR = 19. (d) Single-nanoparticle (25 nm) deposition event with SNR = 10.

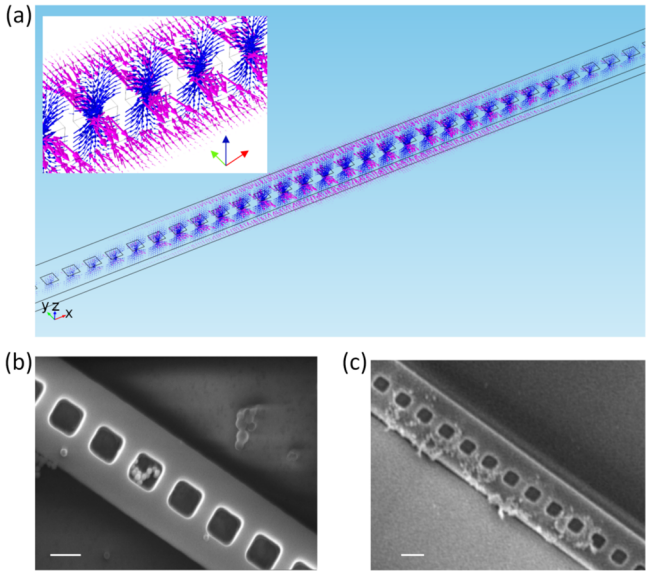

Figure 5. Optical trapping by the resonant cavity. (a) Gradient force vector of the cavity resonance mode. The red line shows the *xy* plane distribution, and the blue line shows the *xz* plane distribution. The force distribution follows a Gaussian profile in the *x* direction, the same as the intensity distribution. Inset shows a zoom-in image of the middle of the cavity. The force vectors indicate that nanoparticles were pulled by the gradient force into the cuboid and then pushed against the side walls, where the electric field intensity maximizes. (b) SEM image of nanoparticles deposited in the center air-square region when the cavity resonance was excited. (c) Nanoparticles deposit randomly along the waveguide when the laser was off. Scale bar: 200 nm.

constant nitrogen flow (pressure 6 psi). Supporting Information Figure S1b verifies that piezospray deposited individual nanoparticles onto a silicon chip. In contrast to the piezospray method, the electrospray transferred more than 3 keV energy ($\sim 10^5 k_B T$) to the nanoparticle (of size 5 nm as an example), even if we assume only one charge was trapped on one nanoparticle. This is much greater than the gradient force trapping energy. A more detailed analysis shows that the electrospray-generated aerosol nanoparticles flew at high speed, on the order of 10^3 m/s (see Supporting Information).[37] Figure 6b and c show the resonance shifts and *Q* shifts for 5 and 1.8 nm gold nanoparticles. Instead of the observed single-step resonance jumps or *Q* drops in Figure 3a and b, distributed resonance shifts were observed. To analyze the statistics, Figure 6d plots the histogram of the resonance shifts, calculated by taking the subtraction of two consecutive resonance shifts in Figure 6b. The distributions fit to Gaussian distributions, because the resonance shift is proportional to the electromagnetic field intensity, and our cavity design generates a Gaussian field distribution.[34] In this case, sizing of 1.8 and 5 nm can be discriminated by the width of the normal distribution. The resonance shift method shows higher sensitivity than the *Q* shift method for small nanoparticles (1.8 nm), consistent with the pizeospray case (Figure 3a and b).

CONCLUSION

In summary, we demonstrate the first ultrahigh *Q*, ultrasmall *V*, air-mode photonic crystal nanobeam cavities in a CMOS platform at telecom wavelength. We demonstrate improvement of detecting nanoscale objects by an order of magnitude (from 20 nm down to 1.8 nm). We note that the hybrid plasmonic–WGM cavity exhibited the same level of sensitivity;[23,24] the advantage of the photonic crystal approach is its scalability and CMOS compatibility. Detecting dielectric nanoparticles was not carried out, since the smallest available polystyrene nanoparticles are about 25 nm in diameter. On the basis of the fact that polystyrene nanoparticles have 4 times smaller polarizability than gold nanoparticles of the same sizes (see Supporting Information), we can estimate the detection limit

DOI: 10.1021/acsphotonics.5b00602
ACS Photonics 2015, 2, 1692–1697

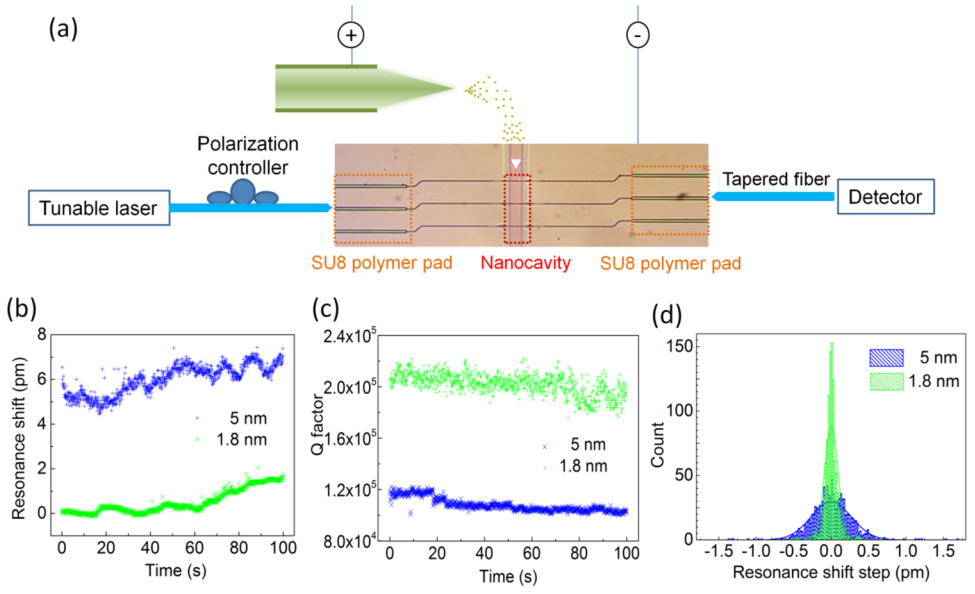

Figure 6. Nanoparticle deposition by electrospray. (a) Schematics of the electrospray-nanobeam setup. The nanobeam cavity was probed the same way as in the piezospray setup. A high voltage (3 kV) was used to generate a Taylor cone and spray the aerosol nanoparticles. The nanoparticles were carried in methanol fluid at 1 μL/min. Nitrogen gas (6 psi) was used to nebulize the aerosol. (b) Resonance shifts and (c) Q drops were measured as nanoparticles of 5 and 1.8 nm were deposited in the cavity with electrospray. Trapping effects were not observed due to the high velocity of the aerosol nanoparticles. (d) Histogram of the resonance shifts in (b).

for a dielectric nanoparticle is about 3 nm in diameter. Therefore, we conclude that the silicon nanobeam cavity, in combination with piezospray or electrospray, can be a research tool or a process analytical tool to perform frequent and rapid size characterization on the limited samples of nanoparticles. Furthermore, the air-mode ultrahigh-Q, ultrasmall-V nanobeam cavity is potentially an ideal platform to enhance the interaction between single molecules, atoms, or solid-state quantum emitters with photons.

■ ASSOCIATED CONTENT

Supporting Information

The Supporting Information is available free of charge on the ACS Publications website at DOI: 10.1021/acsphotonics.5b00602.

Methods used in device fabrication, piezospray and electrospray setup, theoretical analysis of nanoparticle size detection and trapping effects in the piezospray and electrospray configurations (PDF)

■ AUTHOR INFORMATION

Corresponding Author

*E-mail: quan@rowland.harvard.edu.

Notes

The authors declare no competing financial interest.

■ ACKNOWLEDGMENTS

This work was supported by the Rowland Junior Fellowship Program at Rowland Institute at Harvard University. The authors acknowledge helpful discussions with Alessandra Ferzoco at Rowland Institute at Harvard University, Jiangdong Deng and Yuan Lu at the Center for Nanoscale Systems at Harvard University and Cheng Wang at Harvard University. The nanofabrication was performed at the Center for Nanoscale Systems at Harvard University.

■ REFERENCES

(1) Dreaden, E. C.; Austin, L. A.; Mackey, M. A.; El-Sayed, M. A. Size matters: gold nanoparticles in targeted cancer drug delivery. *Ther. Delivery* **2012**, *3*, 457−478.

(2) Petros, R. A.; DeSimone, J. M. Strategies in the design of nanoparticles for therapeutic applications. *Nat. Rev. Drug Discovery* **2010**, *9*, 615−627.

(3) Boisselier, E.; Astruc, D. Gold nanoparticles in nanomedicine: preparations, imaging, diagnostics, therapies and toxicity. *Chem. Soc. Rev.* **2009**, *38*, 1759−1782.

(4) Chen, X.; Zhu, H. Catalysis by Supported Gold Nanoparticles. *Comprehensive Nanoscience and Technology, Vol 3: Nanostructured Surfaces* **2011**, 1−11.

(5) Raimondi, F.; Scherer, G. G.; Kotz, R.; Wokaun, A. Nanoparticles in energy technology: Examples from electrochemistry and catalysis. *Angew. Chem., Int. Ed.* **2005**, *44*, 2190−2209.

(6) Shipway, A. N.; Katz, E.; Willner, I. Nanoparticle arrays on surfaces for electronic, optical, and sensor applications. *ChemPhysChem* **2000**, *1*, 18−52.

(7) Huo, S. D.; Jin, S. B.; Ma, X. W.; Xue, X. D.; Yang, K. N.; Kumar, A.; Wang, P. C.; Zhang, J. C.; Hu, Z. B.; Liang, X. J. Ultrasmall Gold Nanoparticles as Carriers for Nucleus-Based Gene Therapy Due to Size-Dependent Nuclear Entry. *ACS Nano* **2014**, *8*, 5852−5862.

(8) Oh, E.; Delehanty, J. B.; Sapsford, K. E.; Susumu, K.; Goswami, R.; Blanco-Canosa, J. B.; Dawson, P. E.; Granek, J.; Shoff, M.; Zhang, Q.; Goering, P. L.; Huston, A.; Medintz, I. L. Cellular Uptake and Fate of PEGylated Gold Nanoparticles Is Dependent on Both Cell-Penetration Peptides and Particle Size. *ACS Nano* **2011**, *5*, 6434−6448.

(9) Chithrani, B. D.; Ghazani, A. A.; Chan, W. C. W. Determining the size and shape dependence of gold nanoparticle uptake into mammalian cells. *Nano Lett.* **2006**, *6*, 662−668.

(10) Perrault, S. D.; Walkey, C.; Jennings, T.; Fischer, H. C.; Chan, W. C. W. Mediating Tumor Targeting Efficiency of Nanoparticles Through Design. *Nano Lett.* **2009**, *9*, 1909−1915.

(11) Amendola, V.; Meneghetti, M. Size Evaluation of Gold Nanoparticles by UV-vis Spectroscopy. *J. Phys. Chem. C* **2009**, *113*, 4277−4285.

DOI: 10.1021/acsphotonics.5b00602
ACS Photonics 2015, 2, 1692−1697

(12) Haiss, W.; Thanh, N. T. K.; Aveyard, J.; Fernig, D. G. Determination of size and concentration of gold nanoparticles from UV-Vis spectra. *Anal. Chem.* **2007**, *79*, 4215−4221.
(13) Tomaszewska, E.; Soliwoda, K.; Kadziola, K.; Tkacz-Szczesna, B.; Celichowski, G.; Cichomski, M.; Szmaja, W.; Grobelny, J. Detection Limits of DLS and UV-Vis Spectroscopy in Characterization of Polydisperse Nanoparticles Colloids. *J. Nanomater.* **2013**, *2013*, 1−10.
(14) Vollmer, F.; Arnold, S.; Keng, D. Single virus detection from the reactive shift of a whispering-gallery mode. *Proc. Natl. Acad. Sci. U. S. A.* **2008**, *105*, 20701−20704.
(15) Zhu, J. G.; Ozdemir, S. K.; Xiao, Y. F.; Li, L.; He, L. N.; Chen, D. R.; Yang, L. On-chip single nanoparticle detection and sizing by mode splitting in an ultrahigh-Q microresonator (vol 4, pg 46, 2010). *Nat. Photonics* **2010**, *4*, 122−122.
(16) He, L. N.; Ozdemir, K.; Zhu, J. G.; Kim, W.; Yang, L. Detecting single viruses and nanoparticles using whispering gallery microlasers. *Nat. Nanotechnol.* **2011**, *6*, 428−432.
(17) Lu, T.; Lee, H.; Chen, T.; Herchak, S.; Kim, J. H.; Fraser, S. E.; Flagan, R. C.; Vahala, K. High sensitivity nanoparticle detection using optical microcavities. *Proc. Natl. Acad. Sci. U. S. A.* **2011**, *108*, 5976−5979.
(18) Quan, Q. M.; Floyd, D. L.; Burgess, I. B.; Deotare, P. B.; Frank, I. W.; Tang, S. K. Y.; Ilic, R.; Loncar, M. Single particle detection in CMOS compatible photonic crystal nanobeam cavities. *Opt. Express* **2013**, *21*, 32225−32233.
(19) Shao, L. B.; Jiang, X. F.; Yu, X. C.; Li, B. B.; Clements, W. R.; Vollmer, F.; Wang, W.; Xiao, Y. F.; Gong, Q. H. Detection of Single Nanoparticles and Lentiviruses Using Microcavity Resonance Broadening. *Adv. Mater.* **2013**, *25*, 5616−5620.
(20) Mirsadeghi, S. H.; Young, J. F. Ultrasensitive diagnostic analysis of Au nanoparticles optically trapped in silicon photonic circuits at sub-milliwatt powers. *Nano Lett.* **2014**, *14*, 5004−5009.
(21) Ozdemir, S. K.; Zhu, J. G.; Yang, X.; Peng, B.; Yilmaz, H.; He, L.; Monifi, F.; Huang, S. H.; Long, G. L.; Yang, L. Highly sensitive detection of nanoparticles with a self-referenced and self-heterodyned whispering-gallery Raman microlaser. *Proc. Natl. Acad. Sci. U. S. A.* **2014**, *111*, E3836−E3844.
(22) Li, B. B.; Clements, W. R.; Yu, X. C.; Shi, K. B.; Gong, Q. H.; Xiao, Y. F. Single nanoparticle detection using split-mode microcavity Raman lasers. *Proc. Natl. Acad. Sci. U. S. A.* **2014**, *111*, 14657−14662.
(23) Dantham, V. R.; Holler, S.; Barbre, C.; Keng, D.; Kolchenko, V.; Arnold, S. Label-Free Detection of Single Protein Using a Nanoplasmonic-Photonic Hybrid Microcavity. *Nano Lett.* **2013**, *13*, 3347−3351.
(24) Baaske, M. D.; Foreman, M. R.; Vollmer, F. Single-molecule nucleic acid interactions monitored on a label-free microcavity biosensor platform. *Nat. Nanotechnol.* **2014**, *9*, 933−939.
(25) Vollmer, F.; Arnold, S. Whispering-gallery-mode biosensing: label-free detection down to single molecules. *Nat. Methods* **2008**, *5*, 591−596.
(26) Vollmer, F.; Braun, D.; Libchaber, A.; Khoshsima, M.; Teraoka, I.; Arnold, S. Protein detection by optical shift of a resonant microcavity. *Appl. Phys. Lett.* **2002**, *80*, 4057−4059.
(27) Arnold, S.; Khoshsima, M.; Teraoka, I.; Holler, S.; Vollmer, F. Shift of whispering-gallery modes in microspheres by protein adsorption. *Opt. Lett.* **2003**, *28*, 272−274.
(28) Vollmer, F.; Yang, L. Label-free detection with high-Q microcavities: a review of biosensing mechanisms for integrated devices. *Nanophotonics-Berlin* **2012**, *1*, 267−291.
(29) Wang, C.; Quan, Q. M.; Kita, S.; Li, Y. H.; Loncar, M. Single-nanoparticle detection with slot-mode photonic crystal cavities. *Appl. Phys. Lett.* **2015**, *106*.26110510.1063/1.4923322
(30) Deotare, P. B.; McCutcheon, M. W.; Frank, I. W.; Khan, M.; Loncar, M. High quality factor photonic crystal nanobeam cavities. *Appl. Phys. Lett.* **2009**, *94*.12110610.1063/1.3107263
(31) Yang, D. Q.; Kita, S.; Liang, F.; Wang, C.; Tian, H. P.; Ji, Y. F.; Loncar, M.; Quan, Q. M. High sensitivity and high Q-factor nanoslotted parallel quadrabeam photonic crystal cavity for real-time and label-free sensing. *Appl. Phys. Lett.* **2014**, *105*.06311810.1063/1.4867254
(32) Zhang, Y. N.; Bulu, I.; Tam, W. M.; Levitt, B.; Shah, J.; Botto, T.; Loncar, M. High-Q/V air-mode photonic crystal cavities at microwave frequencies. *Opt. Express* **2011**, *19*, 9371−9377.
(33) Quan, Q. M.; Deotare, P. B.; Loncar, M. Photonic crystal nanobeam cavity strongly coupled to the feeding waveguide. *Appl. Phys. Lett.* **2010**, *96*, 20310210.1063/1.3429125.
(34) Quan, Q. M.; Loncar, M. Deterministic design of wavelength scale, ultra-high Q photonic crystal nanobeam cavities. *Opt. Express* **2011**, *19*, 18529−18542.
(35) Hansen, P. M.; Bhatia, V. K.; Harrit, N.; Oddershede, L. Expanding the optical trapping range of gold nanoparticles. *Nano Lett.* **2005**, *5*, 1937−1942.
(36) Jauffred, L.; Taheri, S. M. R.; Schmitt, R.; Linke, H.; Oddershede, L. B. Optical Trapping of Gold Nanoparticles in Air. *Nano Lett.* **2015**, *15*, 4713−4719.
(37) Suh, J.; Han, B.; Okuyama, K.; Choi, M. Highly charging of nanoparticles through electrospray of nanoparticle suspension. *J. Colloid Interface Sci.* **2005**, *287*, 135−140.
(38) Su, J.; Goldberg, A. F. G.; Stoltz, B. M. Label-free detection of single nanoparticles and biological molecules using microtoroid optical resonators. *Light: Sci. Appl.*, in press.

NOTE ADDED IN PROOF

After submitting our work, we became aware of a previewed paper by Su et al., where single nanoparticle 5 nm in diameter was detected using microtoroid resonators.[38]

DOI: 10.1021/acsphotonics.5b00602
ACS Photonics 2015, 2, 1692−1697